Au/TiO_2 Nanosystems: A Combined RF-Sputtering/ Sol−Gel Approach

Lidia Armelao, Davide Barreca,* and Gregorio Bottaro

ISTM-CNR and INSTM, Department of Chemistry, Padova University, Via Marzolo, 1 - 35131 Padova, Italy

Alberto Gasparotto and Eugenio Tondello

Department of Chemistry, Padova University and INSTM, Via Marzolo, 1 - 35131 Padova, Italy

Matteo Ferroni

Physical Chemistry Department and INFM, UdR Venezia, Ca' Foscari Venice University, Via Torino, 155/B - Venezia-Mestre, Italy

Stefano Polizzi

Physical Chemistry Department, Ca' Foscari Venice University, Via Torino, 155/B - Venezia-Mestre, Italy

Received December 16, 2003. Revised Manuscript Received April 28, 2004

An original synthetic approach to Au/TiO_2 nanosystems is developed. The adopted technique is based on the RF-sputtering of gold (*guest*) on porous titania xerogels (*host*) obtained by the sol−gel route. Such a *combined* synthetic pathway joins the peculiarities offered by the features of the sol−gel layers (porosity, nonbridging groups) and the advantages of plasmochemical methods (conformal coverage, infiltration power). In particular, *host* titania substrates were first prepared on silica by dip-coating from ethanolic solutions of $Ti(OPr^i)_4$ (OPr^i=*iso*-propoxy) and Hacac (2,4-pentanedione). Subsequently, Au depositions were performed on the *as-prepared* xerogels in Ar plasmas at low temperatures. The resulting samples were finally annealed in air between 200 and 600 °C with the aim of tailoring the system features as a function of thermal treatment and gold content. Their structural, compositional, and morphological evolution was investigated by Glancing Incidence X-ray Diffraction (GIXRD), Transmission Electron Microscopy (TEM), optical absorption spectroscopy, X-ray Photoelectron Spectroscopy (XPS), and Atomic Force Microscopy (AFM). The adopted strategy enabled the synthesis of Au/TiO_2 nanosystems with characteristics strongly dependent on the deposited gold amount and processing conditions. In this way, materials with tunable structure, composition, and optical properties could be synthesized.

Introduction

Au/TiO_2 nanosystems have come under intense scrutiny for a broad range of applications thanks to their intriguing chemico-physical properties. Such unique characteristics are derived from phenomena occurring at the Au nanoparticle/TiO_2 matrix interface, which represent an interesting example of weak Au/TiO_2 interactions.[1,2] The latter play a key role in promoting the catalytic activity of such systems for a variety of processes,[3−6] including CO oxidation to CO_2,[7−9] NO_x reduction to N_2,[10] and water gas shift reaction.[11,12] Further interest toward Au/TiO_2 nanosystems is addressed to their use in nonlinear optical devices,[13−16]

* Corresponding author phone: +39-0498275170; fax: +39-0498275161; e-mail: davide@chin.unipd.it.

(1) Persuad, R.; Madey, T. E. *The Chemical Physics of Solid Surfaces and Heterogeneous Catalysis*; King, D. A., Woodruff, D. P., Eds., Vol. 8, Elsevier: Amsterdam, 1997.
(2) Vittadini, A.; Selloni, A. *J. Chem. Phys.* **2002**, *117*, 353.
(3) Wolf, A.; Schüth, F. *Appl. Catal., A* **2002**, *226*, 1.
(4) Mavrikakis, M.; Stoltze, P.; Norsokov, J. K. *Catal. Lett.* **2000**, *64*, 101.
(5) Iizuka, Y.; Fujiki, H.; Yamuachi, N.; Chijiiwa, T.; Arai, S.; Tsubota, S.; Haruta, M. *Catal. Today* **1997**, *36*, 115.
(6) Wang, C.-y.; Liu, C.-y.; Chen, J.; Shen, T. *J. Colloid Interface Sci.* **1997**, *191*, 464.
(7) Haruta, M. *Catal. Today* **1997**, *36*, 153.
(8) Okumura, M.; Nakamura, S.; Tsubota, S.; Nakamura, T.; Azuma, M.; Haruta, M. *Catal. Lett.* **1998**, *51*, 53.
(9) Okazaki, K.; Morikawa, Y.; Tanaka, S.; Ichikawa, S.; Tanaka, K.; Kohyama, M. *Mater. Res. Soc. Symp. Proc.* **2003**, *738*, G13.7.1.
(10) Valden, M.; Goodman, D. W. *Isr. J. Chem.* **1998**, *38*, 285.
(11) Sakurai, H.; Ueda, A.; Kobayashi, T.; Haruta, M. *Chem. Commun.* **1997**, 271.
(12) Zhang, L.; Cosandey, F.; Persuad, R.; Madey, T. E. *Surf. Sci.* **1999**, *439*, 73.
(13) Cattaruzza, E. *Nucl. Instrum. Methods Phys. Res., Sect. B* **2000**, *169*, 141.
(14) Deki, S.; Aoi, Y.; Yanagimoto, H.; Ishii, K.; Akamatsu, K.; Mizuhata, M.; Kajinami, A. *J. Mater. Chem.* **1996**, *6*, 1879 and references therein.
(15) Shinojima, H.; Yumoto, J.; Uesugi, S. *Appl. Phys. Lett.* **1992**, *60*, 298.

10.1021/cm0353308 CCC: $27.50
Published on Web 07/31/2004

thanks to the high $\chi^{(3)}$ values related to the high polarizability of the gold particles (*guest*) and the high dielectric constant of the titania matrix (*host*).[17,18] Moreover, a great attention has been focused on the use of Au/TiO_2 in photoelectrochemical solar cells, due to the photocatalytic properties of TiO_2[19,20] that are further enhanced by gold dispersion.[21] Dye-sensitized nanocrystalline TiO_2 solar cells have achieved sunlight-to-electrical power conversion efficiencies greater than 9% and photocurrents >16 mA $\times$ cm^{-2}.[22]

As a general rule, the functional performances of Au/TiO_2 materials are strongly dependent on the Au particle size and distribution and hence on the adopted synthetic procedure.[3,23] Generally, these systems have been prepared by both physical and chemical routes, including ion implantation,[24] ionized cluster beam,[25] evaporation,[10,12,26,27] sputtering,[16,18,28,29] Chemical Vapor Deposition (CVD),[8] wet chemical methods,[7,14,30] and sol−gel (SG) routes.[6,23,31,32] Nonetheless, no reports concerning the *combined* use of different preparation techniques for the gold *guest* particles and the titania *host* phase have appeared in the literature up to date.

In the present work, Au/TiO_2 nanosystems were synthesized by an original *hybrid* technique aimed at the control of the peculiar properties exhibited by gold-titania at the nanometric scale. Based on our recent studies concerning the preparation of CeO_2-ZrO_2 nanosystems by a Plasma-Enhanced CVD/SG approach,[33] the attention was focused on the dispersion of Au nanoparticles by RF-sputtering on porous titania xerogels prepared by the SG technique and on subsequent thermal treatments of the obtained systems. To the best of our knowledge, only a previous report concerning the preparation of $Ag-SiO_2$ composites by a combined Pulsed Laser Deposition/SG approach has appeared in the literature up to date.[34]

The main advantages of a plasma/liquid phase *hybrid* approach have already been discussed.[33] In particular, the peculiar characteristics of RF-sputtering are the flexibility that permits the fabrication of composite films of various metals and dielectric materials and the capability to produce uniformly distributed metal clusters.[35,36] Moreover, the synergic competition between deposition/ablation phenomena characterizing sputtering processes from glow discharges is a key step in order to obtain nanoparticles with tailored size and distribution. In these processes, plasma activation of both gas-phase species and growth surface can induce intermixing processes between the *host* matrix and the *guest* phase. Such effects are further enhanced by the properties of $TiO_x(OH)_y(OR)_z$ xerogels, i.e., the porous structure and the presence of *nonbridging groups* (−OH and −OR), allowing, in principle, an optimal dispersion of the deposited gold particles. These features might result in unexpected and/or improved functional properties. In the present case, due to the soft conditions adopted for Au deposition, mild plasmochemical modifications of the xerogel properties are expected to involve essentially the outermost sample region. Ex-situ thermal treatments could induce either a coalescence of the gold particles in the near-surface region or their migration in the inner layers of the *host* titania matrix. Moreover, an important advantage of the proposed synthetic pathway is its versatility and feasibility for the preparation of a wide range of *host/guest* metal/metal oxide systems, featuring properties hardly attainable by conventional synthetic routes.

In the present work, RF-sputtering of gold was performed on SG titania xerogels at temperatures as low as 60 °C, to avoid thermally induced modifications of the xerogel morphology and structure. The obtained samples were subsequently annealed in air for 1 h at temperatures ranging from 200 to 600 °C.

Film nanostructure, composition, and morphology were investigated by GIXRD, TEM, optical absorption, XPS, and AFM in order to analyze the system evolution as a function of gold content and annealing conditions.

Experimental Section

Synthesis. Titania xerogels were deposited on Herasil silica slides (Heraeus, Quarzschmelze, Hanau, Germany) 1 cm $\times$ 2 cm $\times$ 1 mm each, cleaned by a previously optimized procedure[37] aimed at removing organic residuals. The xerogels were prepared by dip-coating from ethanolic (C_2H_5OH, Carlo Erba, 99.8%) solutions of $Ti(OPr^i)_4$ (ABCR, 97%) and Hacac (Aldrich, 99+ %) ($C(TiO_2) \approx 50$ g/L; $Ti(OPr^i)_4$:Hacac = 2:1), at a withdrawal speed of ≈ 12 cm$\times$min^{-1}. All the *as-prepared* specimens resulted well adherent to the substrate, pale yellow colored, homogeneous, crack free and without any detectable crystalline phase, as proved by GIXRD analyses. The xerogels were used in the subsequent RF-sputtering experiments without further treatments.

Au depositions on titania xerogels were performed by a custom-built Radio Frequency (RF) Plasmochemical reactor (ν

(16) Quélin, X.; Sakars, J.; Bourdon, A.; Gadenne, P. *Physica B* **2000**, *279*, 102.
(17) Hache, F.; Ricard, D.; Flytzanis, C. *J. Opt. Soc. Am. B: Opt. Phys.* **1986**, *3*, 1647.
(18) Maruyama, O.; Senda, Y.; Omi, S. *J. Non-Cryst. Solids* **1999**, *259*, 100.
(19) Hagfeldt, A.; Grätzel, M. *Acc. Chem. Res.* **2000**, *33*, 269.
(20) Prokes, S. M.; Carlos, W. E.; Gole, J. L.; She, C.; Lian, T. *Mater. Res. Soc. Symp. Proc.* **2003**, *738*, G8.9.1.
(21) Chandrasekharan, N.; Kamat, P. V. *J. Phys. Chem. B* **2000**, *104*, 10851.
(22) Cherepy, N. J.; Smestad, G. P.; Grätzel, M.; Zhang, J. Z. *J. Phys. Chem. B* **1997**, *101*, 9342.
(23) Innocenzi, P.; Brusatin, G.; Martucci, A.; Urabe K. *Thin Solid Films* **1996**, *279*, 23.
(24) Fukumi, K.; Chayahara, A.; Kadono, K.; Sakaguchi, T.; Horino, Y.; Miya, M.; Fujii, K.; Hayakawa, J. *J. Appl. Phys.* **1994**, *75*, 3075.
(25) Takaoka, G. H.; Hamano, T.; Fukushima, K.; Matsuo, J.; Yamada, I. *Nucl. Instrum. Methods Phys. Res., Sect. B* **1997**, *121*, 503.
(26) Guo, Q.; Luo, K.; Davis, K. A.; Goodman, D. W. *Surf. Interface Anal.* **2001**, *32*, 161.
(27) Parker, S. C.; Grant, A. W.; Bondzie, W. A.; Campbell, C. T. *Surf. Sci.* **1999**, *441*, 10.
(28) Sasaki, T.; Koshizaki, N.; Koinuma, M.; Matsumoto, Y. *Nanostruct. Mater.* **1999**, *12*, 511.
(29) Yoon, J.-W.; Sasaki, T.; Koshizaki, M.; Traversa, E. *Scripta Mater.* **2001**, *44*, 1865.
(30) Chuanyi, W.; Chunyan, L.; Tao, S. *Chin. Sci. Bull.* **1998**, *43*, 210.
(31) Lee, M.; Chae, L.; Lee, K. C. *Nanostruct. Mater.* **1999**, *11*, 195.
(32) Epifani, M.; Giannini, C.; Tapfer, L.; Vasanelli, L. *J. Am. Ceram. Soc.* **2000**, *83*, 2385.
(33) Armelao, L.; Barreca, D.; Bottaro, G.; Gasparotto, A.; Tondello, E.; Ferroni, M.; Polizzi, S. *Chem. Vap. Deposition*, in press.
(34) Renard, C.; Ricolleau, C.; Fort, E.; Besson, S.; Gacoin, T.; Boilot, J.-P. *Appl. Phys. Lett.* **2002**, *80*, 300.
(35) Liao, H. B.; Xiao, R. F.; Fu, J. S.; Yu, P.; Wong, G. K. L.; Sheng, P. *Appl. Phys. Lett.* **1997**, *70*, 1.
(36) Cho, S.; Lee, S.; Oh, S. G.; Park, S. J.; Kim, W. M.; Cheong, B. K.; Chung, M.; Song, K. B.; Lee, T. S.; Kim, S. G. *Thin Solid Films* **2000**, *377*, 97.
(37) Armelao, L.; Bertoncello, R.; Coronaro, S.; Glisenti, A. *Sci. Technol. Cultural Heritage* **1998**, *7*, 41.

= 13.56 MHz)[38] using electronic grade Ar (purity 5.0) as plasma source. A 2" diameter gold target (0.1 mm thick; BALTEC AG, 99.99%) was fixed on the RF electrode, while the substrates were placed on a second grounded electrode whose temperature was measured by a thermocouple inserted into the resistively heated sample holder. Depositions were carried out at 60 °C substrate temperature with an electrode-to-electrode distance of 50 mm, under optimized conditions. The resulting nanosystems were analyzed both *as-prepared* and after 1 h ex-situ annealing at 200, 400, and 600 °C in air.

Characterization. Glancing-Incidence XRD patterns were recorded by means of a Bruker D8 Advance diffractometer equipped with a Göbel mirror and a CuKα source (40 kV, 40 mA), at a fixed incidence angle of 1.5°. The average crystallite dimensions were estimated by means of the Scherrer equation. For the Au crystallites, this analysis was performed using the peak related to (200) planes ($2\vartheta = 44.5°$), instead of the most intense one ($2\vartheta = 38.4°$, (111)) due to the overlap with TiO_2 *anatase* (112) reflections at $2\vartheta = 38.6°$ for samples annealed at $T \geq 400$ °C.

TEM images were taken with a JEOL 3010, operating at 300 kV, equipped with a Gatan slowscan CCD camera (Mod. 794) and an Oxford Instrument EDS microanalysis detector (Mod. 6636). The samples for cross-section observations were obtained by means of mechanical grinding, dimpling, and low-angle Ar^+ ion milling.

Optical absorption spectra of the films were recorded in the range 300−800 nm on a Cary 5E (Varian) UV−vis−NIR dual-beam spectrophotometer with a spectral bandwidth of 1 nm. In each spectrum, the silica substrate contribution was subtracted.

XPS spectra were run on a Perkin-Elmer Φ 5600ci spectrometer at a pressure lower than 10^{-9} mbar, using a standard AlKα excitation source (1486.6 eV). The spectrometer was calibrated by assigning to the $Au4f_{7/2}$ line the Binding Energy (BE) of 84.0 eV with respect to the Fermi level. The residual BE shifts were corrected assigning to the C1s line of adventitious carbon a value of 284.8 eV.[39] The estimated BEs standard deviation was ±0.2 eV. After a Shirley-type background subtraction,[40] the raw spectra were fitted using a nonlinear least-squares deconvolution program. The atomic compositions were evaluated using sensitivity factors provided by Φ V5.4A software. Depth profiles were carried out by an Ar^+ beam at 2.5 kV with an argon partial pressure of $\approx 5 \times 10^{-8}$ mbar and a rastered area of 2×2 mm^2. Samples were introduced directly into the analysis chamber by a fast entry lock system. The sample thickness was evaluated by measuring the depth of the erosion crater at the end of each profile by means of a Tencor Alpha Step profiler.

AFM micrographs were recorded by a Park Autoprobe CP instrument operating in contact mode and in air. The background was subtracted from the images using the ProScan 1.3 software by Park Scientific. Images were recorded in different sample areas in order to check surface homogeneity.

Results and Discussion

Table 1 summarizes the preparation conditions of the synthesized gold-titania nanosystems. Three different sample sets (**1**→**3**) with different V_{bias} values were prepared to vary the overall sputtered gold amount and, hence, the morphological and structural properties of the prepared nanosystems, with particular attention to clusterlike or islandlike systems. Using the working conditions in Table 1, all the *as-prepared* samples were homogeneous, crack-free, and their color depended on the synthesis conditions, changing from green to blue and, finally, pink on going from set **1** to set **3**. These color changes could be attributed to charge separation and, in particular, to a progressive electron transfer from titania to gold nanoparticles. For each deposition condition, one of the specimens was analyzed *as-prepared* (**A**), while the remaining three were characterized after annealing ex-situ at 200 (**B**), 400 (**C**), and 600 °C (**D**).

Table 1. Synthesis Conditions for Au/TiO₂ Nanosystems[a]

sample		*t* (min)	RF power (W)	*p* (mbar)	V_{bias} (V)	thermal treatment (°C)
set 1	1A	10	25	0.380	−550	as-prepared
	1B					200
	1C					400
	1D					600
set 2	2A	10	5	0.080	−305	as-prepared
	2B					200
	2C					400
	2D					600
set 3	3A	20	5	0.380	−250	as-prepared
	3B					200
	3C					400
	3D					600

[a] In all cases, annealing was performed for 1 h in air. Typical film thickness was ≈60 nm.

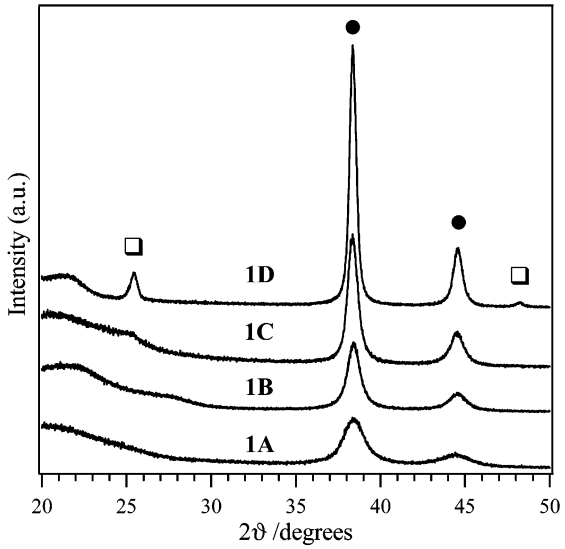

Figure 1. GIXRD patterns of Au/TiO_2 nanosystems belonging to set **1**. Peak positions for *anatase* TiO_2 (□) and Au (●) are indicated.

Microstructural Characterization. Preliminary GIXRD investigations were performed on *as-prepared* titania xerogels subjected to an Ar plasma treatment (RF power=25 W, total pressure=0.380 mbar, deposition time=10′), to investigate the eventual crystallization of TiO_2 matrices. In this case, no diffraction peaks were observed. On the other hand, after ex-situ annealing in air at $T \geq 400$ °C for 1 h, reflections attributable to TiO_2 in the *anatase* form[41] were clearly detectable, as typically observed in the initial phases of SG titania crystallization.[29,31,32,42]

As an example, Figure 1 displays the GIXRD spectra of Au/TiO_2 samples belonging to set **1**. Only two reflections located at $2\vartheta = 38.4°$ and $2\vartheta = 44.5°$ were detected up to an annealing temperature of 200 °C (**1A**, **1B**) and ascribed to the (111) and (200) planes of *fcc* metallic Au.[43] An increase in the treatment temperature resulted in an intensity enhancement and narrowing of these

(38) Barreca, D.; Gasparotto, A.; Tondello, E.; Sada, C.; Polizzi, S.; Benedetti, A. *Chem. Vap. Deposition* **2003**, *9*, 199.
(39) Briggs, D.; Seah, M. P. *Practical Surface Analysis*, John Wiley: Chichester, Vol. 1, 1990.
(40) Shirley, D. A. *Phys. Rev.* **1972**, *55*, 4709.

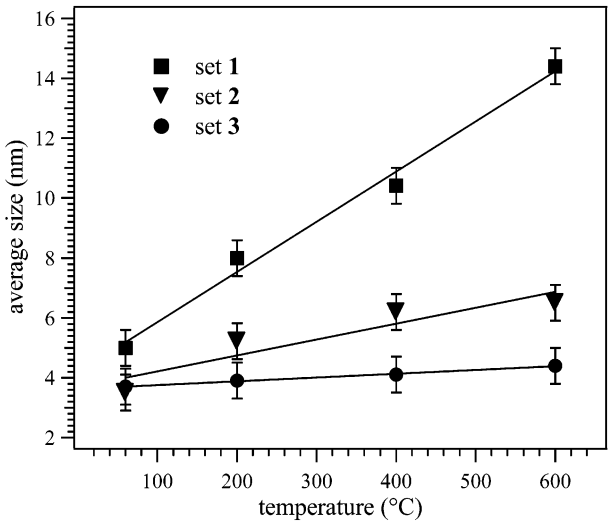

Figure 2. Dependence of gold crystallite size on annealing temperature for Au/TiO_2 nanosystems. The 60 °C temperature corresponds to the *as-prepared* specimens.

peaks, indicating a progressive growth of gold particles. The appearance of signals at $2\vartheta \approx 25.3°$ (101) and 48.0° (200) after annealing at 600 °C (Figure 1, **1D**) was ascribed to the crystallization of *anatase* TiO_2, with an average size of ≈15 nm.

As a general trend, the mean Au nanocrystal dimensions (Figure 2) increased linearly with annealing temperature, indicating a progressive coalescence of gold agglomerates. However, the curve slope increases with the overall Au amount, i.e**.** from set **3**, where the nanocrystal size shows a very weak dependence on temperature, to set **1** (Figure 2), where crystallites increase from 5 to 15 nm from the *as-prepared* specimen (60 °C) to the 600 °C-annealed one. Such a behavior can be interpreted by assuming a dependence of particle coalescence on the overall sputtered gold amount, as explained below.

A deeper insight into the system nanostructure as a function of thermal treatment was obtained by TEM analyses on two selected samples, **2A** (*as-prepared*) and **2D** (annealed at 600 °C, 1 h). A cross-section TEM image of specimen **2A** is shown in Figure 3(a), together with a High Resolution (HR) HRTEM image (Figure 3(b)). It can be seen that on the titania film surface two kinds of Au particles are deposited. The smallest ones have sizes lower than 2 nm, whereas the largest particles range between 5 and 8 nm. The number of smaller particles seems to be much higher than that of the larger ones. This feature might be attributed to *host* matrix effects, i.e., the presence of −OH and −OR polar groups in the titania xerogels, acting as grafting sites for the sputtered gold particles. This feature, together with the soft processing conditions (deposition temperature=60 °C), is likely to result in the formation of many nucleation sites per unit area, that limit the subsequent particle aggregation. Concerning the larger particles, an inspection of the HRTEM image in Figure 3(b) allows for discerning the (111) planes of *fcc* metal gold. In

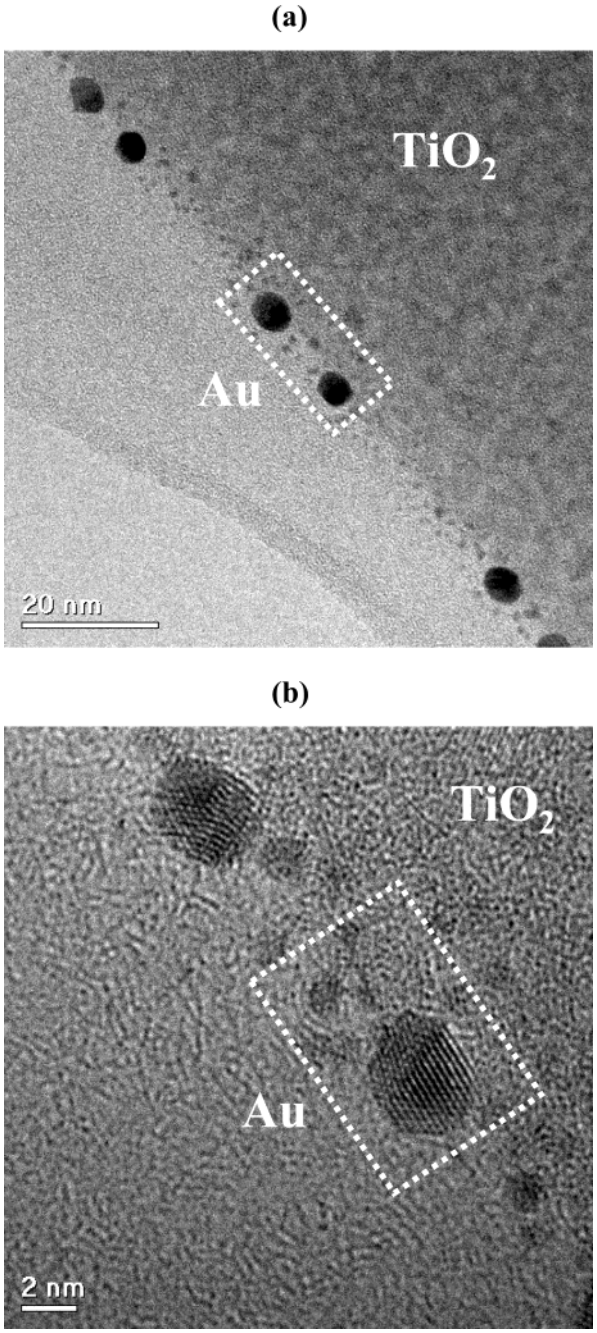

Figure 3. (a) TEM image of the *as-prepared* set **2** sample (**2A**); (b) HRTEM of the same sample.

agreement with GIXRD results, the titania matrix resulted in amorphous.

As a matter of fact, a significant structural evolution is observed upon thermal treatment in air. In Figure 4 a TEM image (a) and two HRTEM ones ((b) and (c)) of the sample annealed at 600 °C (**2D**) are shown. It may be seen that the effect of the annealing is the crystallization of the titania *host* matrix (fringes due to (101) *anatase* planes are evident) and the growth of larger gold particles at expenses of smaller ones, which almost disappear in this sample. Moreover, the aggregation of different Au nanocrystallites can be observed. Such phenomena were further confirmed by optical absorption spectroscopy, that revealed a marked evolution for samples belonging to the different sets as a function of the annealing temperature. As an example, Figure 5

(41) *Pattern* No. 21−1272, *JCPDS* 2000.
(42) Okada, K.; Yamamoto, N.; Kameshima, Y.; Yasumori, A.; MacKenzie, K. J. D., *J. Am. Ceram. Soc.* **2001**, *84*, 1591.
(43) *Pattern* No. 4−784, *JCPDS* 2000.

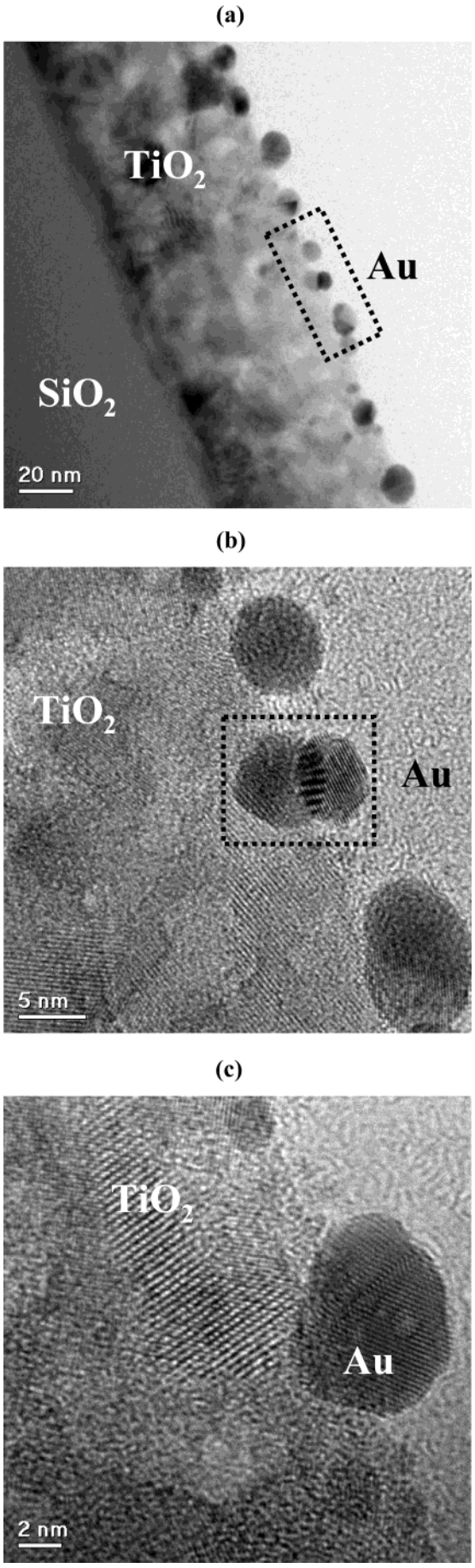

Figure 4. (a) TEM image of the set **2** sample annealed at 600 °C (**2D**); (b) and (c) HRTEM images of the same sample.

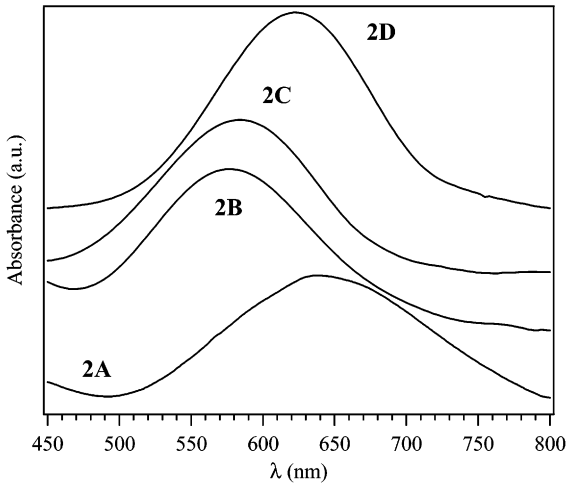

Figure 5. Optical absorption spectra of Au/TiO_2 nanosystems belonging to set **2** as a function of annealing temperature.

displays the optical spectra in the visible range for set **2** specimens. The absorption spectrum of the *as-prepared* Au/TiO_2 nanosystems showed a broadened band centered at $\lambda \approx 640$ nm and extending toward the IR region. Such an absorption, responsible for the observed blue coloration, was typical for an Au/TiO_2 nanosystem with a very broad particle size distribution.[21] On increasing the treatment temperature up to 200 °C, the development of a Surface Plasmon Resonance (SPR) peak centered at ≈590 nm, typical for gold nanoclusters dispersed in/on a titania matrix, was observed.[14,31,32] The plasmon band increased in intensity and shifted to longer wavelengths, up to ≈630 nm, with increasing heat-treatment temperature. A similar behavior, that is consistent with the specimen color change from blue (*as-prepared*) to purplish (600 °C-annealed), have already been reported for gold-dispersed glasses synthesized by liquid-phase routes.[14] The observed SPR peak shift of ≈40 nm toward longer wavelengths was mainly attributed to the change in the relative permittivity of the *host* titania matrix due to the crystallization process.[6,30−32,36,44−47] Moreover, the relatively broad absorptions are likely to indicate that the matrix not only serves as an environment providing the dielectric character but also interacts with Au nanoparticles to some extent.[31]

The evolution of the SPR peak on increasing annealing temperature can also be related to gold distribution variations in the surface and near-surface layers upon thermal treatment (see below). In fact, as shown by TEM investigations, after annealing at 600 °C (sample **2D**, Figure 4) gold nanoparticles grow larger and become essentially isolated and surrounded by the *host* titania matrix.

Surface and In-Depth Composition. All XPS surface spectra displayed the main photopeaks of C, O, Au, and Ti. Samples annealed at $T < 400$ °C showed the presence of carbon throughout the film thickness, indicating that such thermal treatments were not successful for a complete TiO_2 network formation. Such an hypothesis was confirmed by observing the evolution of O1s signal, which could be fitted by three components at 530.0, 531.6, and 533.0 eV, ascribed to lattice oxygen in Ti(IV) oxides, adsorbed −OH groups and H_2O, respectively.[33,48] For $T > 400$ °C, the latter two components underwent an appreciable decrease.

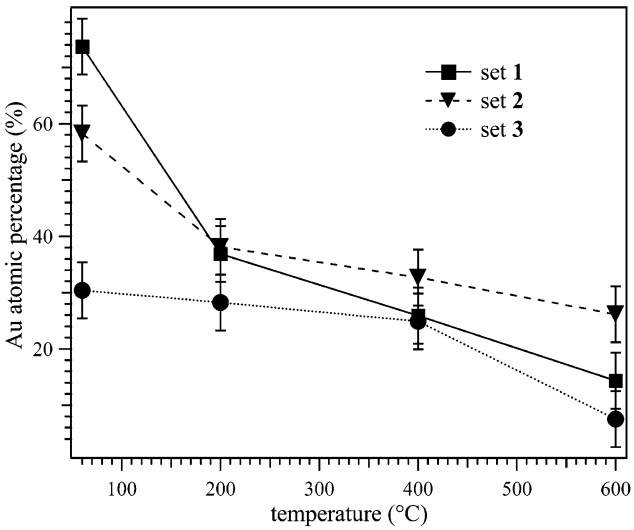

Figure 6. Dependence of Au surface percentage (as determined by XPS) on annealing temperature for Au/TiO_2 nanosystems belonging to set **1**, **2**, and **3**. Quantifications were made taking into account only Au, Ti, and O in order to avoid undesired data alterations due to the presence of surface adventitious carbon in variable amounts for different specimens.

Whatever the annealing conditions, the $Ti2p_{3/2}$ BE was always close to 459.0 eV, in agreement with literature values for Ti(IV).[48−50] The $Au4f_{7/2}$ component was centered at 84.0 eV for all specimens, as expected for metallic gold.[14,48,51−54]

For all three sample sets, a progressive decrease of Au surface amount was observed upon annealing (Figure 6). Nevertheless, the dependence of Au percentage on temperature became progressively weaker on going from set **1** to set **3** specimens. This trend was explained by taking into account that the coalescence/agglomeration of gold nanoparticles, favored by an increase of thermal energy,[36,45−47] might be responsible for a diminished surface coverage at higher treatment temperatures, resulting in an apparent lowering of Au percentage. Such a phenomenon was expected to be more effective for nanosystems characterized by a higher gold content (Figure 6, set **1**). Moreover, a further contribution arising from Au penetration in the subsurface layers could not be excluded. Such transformations are likely to be further enhanced at $T > 400$ °C by the structural reorganization accompanying TiO_2 crystallization process.[32,55] Concerning samples belonging to set **3**, the weaker variations of Au surface percentage with the heating temperature were related to the lower gold amount, resulting in a more limited coalescence process. In this case, appreciable Au content variations began to occur at 400 °C, in concomitance with titania crystallization.

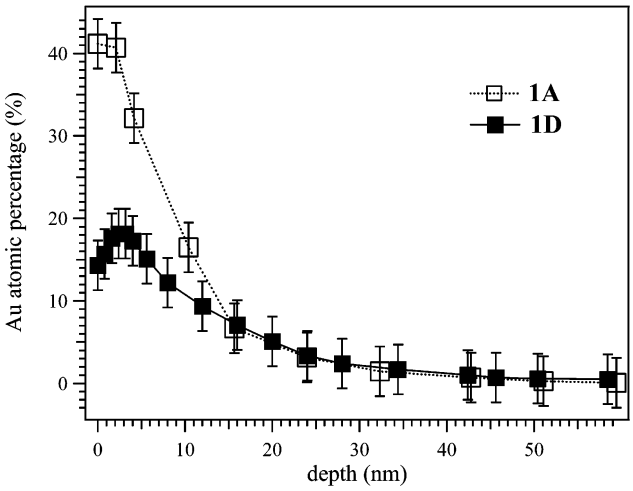

Figure 7. Au XPS depth profiles for samples **1A** (*as-prepared*) and **1D** (annealed at 600 °C, 1 h) (see Table 1). Quantifications were made taking into account Au, Ti, C, and O.

It is worthwhile observing that RF-sputtering of gold on commercial silica slides under the same conditions adopted for set **1** and set **2** samples led to a surface gold content of ≈50%, for *as-prepared* samples, while specimens **1A** and **2A** presented an Au amount of ≈75% and 60%, respectively. A similar difference emphasizes the role of the *host* titania matrix as *regulator* of gold distribution, inducing a different morphology with respect to that observed on other substrates.

Figure 7 compares the gold depth profiles for the *as-prepared* (**1A**) and 600 °C-treated specimens (**1D**). For sample **1A**, Au percentage decreased from ≈40% on the surface to a disappearance at ≈30 nm depth. This behavior, suggesting a gold penetration in inner layers of the titania xerogel at temperatures as low as 60 °C, might be related to the synergy between the xerogel porosity and the infiltration power typical of plasmochemical methods (see above), which, in turn, is favored by the bombarding action exerted by plasma particles. A remarkable modification of the gold profile was observed after treatment at 600 °C (**1D**) that resulted in an apparent lower average Au amount (Figure 7). As previously discussed, this effect could be mainly traced back to a thermally induced gold redistribution in the surface and near-surface layers due to particle agglomeration, whose entity is further increased by TiO_2 crystallization.[32,55] In both cases, the maximum Au penetration depth into the matrix was estimated to be ≈20 nm. A similar thermal evolution was observed also in the XPS depth profiles of specimen belonging to the other sets (Table 1).

At variance with results obtained for CeO_2-ZrO_2 nanosystems,[33] no further gold penetration with respect to the *as-prepared* sample was induced by thermal treatment (compare the two depth profiles in Figure 7).

(44) Kreibig, U.; Vollmer, M. *Optical Properties of Metal Clusters*; Springer-Verlag: Berlin, 1995.
(45) Ishikawa, H.; Ida, T.; Kimura, K. *Surf. Rev. Lett.* **1996**, *3*, 1153.
(46) Schiestel, S.; Cotell, C. M.; Carosella, C. A.; Grabowski, K. S.; Hubler, G. K. *Nucl. Instrum. Methods Phys. Res., Sect. B* **1997**, *127*, 566.
(47) Cai, W. P.; Hofmeister, H.; Rainer, T.; Chen, W. *J. Nanopart. Res.* **2001**, *3*, 443.
(48) Moulder, J. M.; Stickle, W. F.; Sobol, P. E.; Bomben, K. D. *Handbook of X-ray Photoelectron Spectroscopy;* Perkin-Elmer Corporation: Eden Prairie, MN, 1992.
(49) Saied, S. O.; Sullivan, J. L.; Choudhury, T.; Pearce, C. G. *Vacuum* **1988**, *38*, 917.
(50) Slinkard, W. E.; Degroot, P. B. *J. Catal.* **1981**, *68*, 423.
(51) Seah, M. P.; Smith, G. C.; Anthony, M. T *Surf. Interface Anal.* **1990**, *15*, 293.
(52) Anthony, M. T.; Seah, M. P. *Surf. Interface Anal.* **1984**, *6*, 95.
(53) Johansson, G.; Hedman, J.; Berndtsson, A.; Klasson, M.; Nilsson, R. *J. Electron Spectrosc. Relat. Phenom.* **1973**, *2*, 295.
(54) McLean, W.; Colmenares, C. A.; Smith, R. L.; Somorjai, G. A. *J. Phys. Chem.* **1983**, *87*, 788.
(55) Mosaddeq-ur-Rahman, Md.; Yu, G.; Krishna, K. M.; Soga, T.; Watanabe, J.; Jimbo, T.; Umeno, M. *Appl. Opt.* **1998**, *37*, 691.

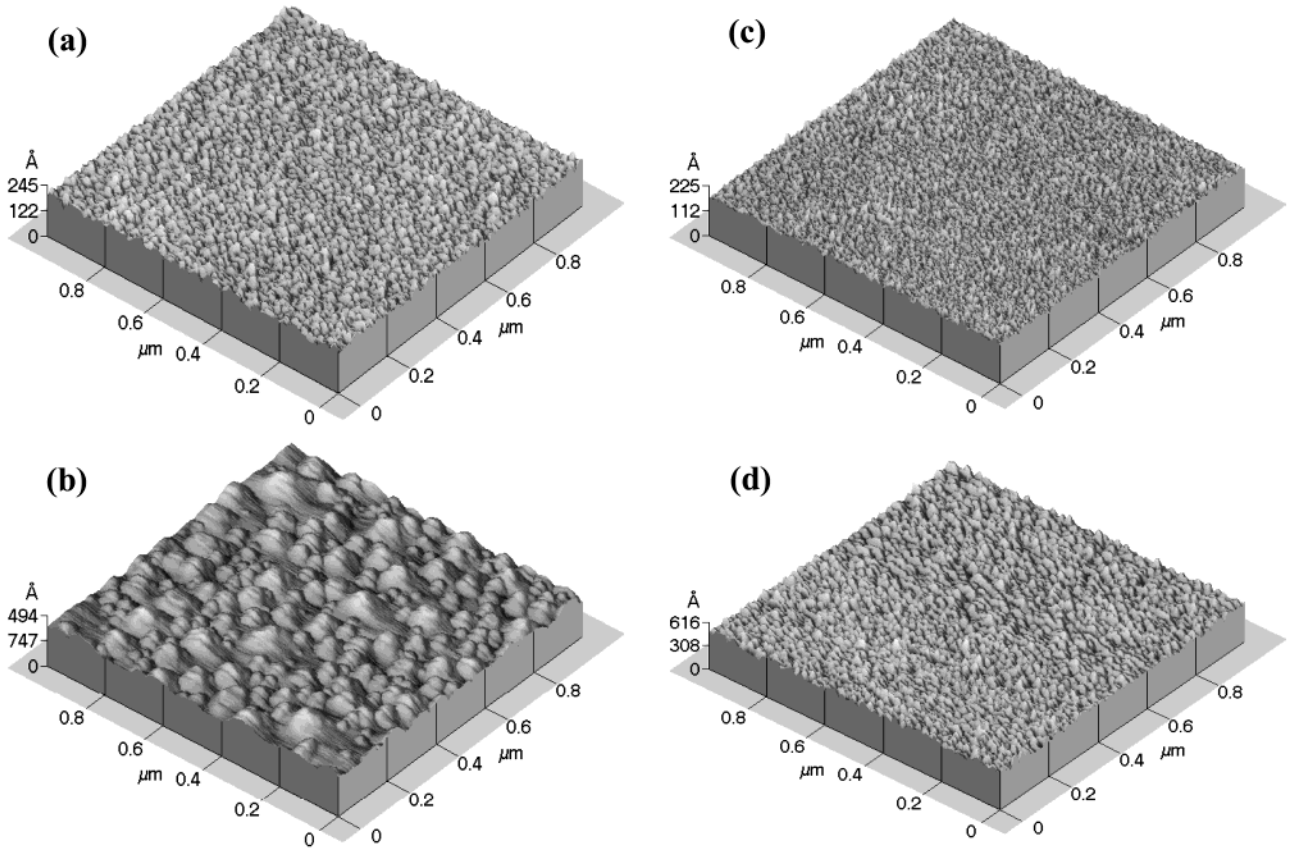

Figure 8. Representative AFM surface micrographs (1×1 μm^2) of specimens **1A** (a), **1D** (b), **2A** (c), **2D** (d).

This difference might be ascribed to the absence of significant *host-guest* interactions, differently from the case of CeO_2-ZrO_2 nanocomposites, where annealing in air produced the formation of a solid solution $Ce_{1-x}Zr_xO_2$.

Morphology. The morphological evolution under annealing was appreciably influenced by the deposition conditions, i.e., the total gold content. Such differences are exemplified in Figure 8, that reports representative AFM images for selected set **1** and **2** samples. In all cases, a typically globular surface texture was detected. The most remarkable variations took place for samples **1A** and **1D**. While for the *as-prepared* specimen (**1A**, Figure 8(a)) the average RMS roughness and grain size were 0.5 and 20 nm, respectively, after 600 °C annealing these values increased to 2 and 60 nm, corresponding to a rougher surface and a less regular morphology (**1D**, Figure 8(b)). Such variations were attributed both to the *host* matrix crystallization processes and to the coalescence of gold agglomerates, as previously discussed. Concerning Au/TiO_2 nanosystems belonging to set **2**, no significant differences in the morphology of the *as-prepared* specimens were observed with respect to set **1** (compare Figure 8(a) and (c)). Thermal treatment at 600 °C produced an increase of the average grain size from 20 to 30 nm, but the observed variations were not as marked as those revealed for set **1** specimens (compare Figure 8(b) and 8(d)). As already pointed out, this different behavior was related to the overall gold content in the *as-prepared* samples belonging to set **1** and set **2**.

The above results suggest that the chemico-physical properties of Au/TiO_2 nanosystems belonging to sets **1**→**3** are strongly influenced by the overall gold amount in the corresponding *as-prepared* specimens, resulting in different Au particles distributions. Concerning set **3** samples, that contain the lowest Au amount, small gold nanoparticles can be considered homogeneously dispersed on the xerogel surface and partially trapped in the matrix pores, so that annealing processes cannot induce appreciable coalescence of Au agglomerates. At progressively higher gold contents (set **2** and **1**), the overall contact area between different Au particles is likely to increase, so that thermally induced coalescence/agglomeration processes are subsequently favored. Such features can explain the different dependence of nanocrystal size on temperature (Figure 2), which resulted appreciably steep for set **1** and very weak for set **3** samples. As a matter of fact, gold nanocrystal size for the *as-prepared* samples resulted ≈4 nm irrespective of the synthesis conditions (Figure 2). Consequently, the principal effects influencing the system evolution were dictated by the Au amount which, in turn, could be controlled by the RF-sputtering parameters. In particular, the entity of Au coalescence/agglomeration processes, decreasing from set **1** to **3,** was also responsible for the observed evolution of optical, compositional, and morphological properties.

Conclusions

In this work, Au/TiO_2 nanosystems were synthesized by an original *hybrid* route, consisting in the RF-sputtering of gold (*guest*) onto titania xerogels (*host*) and subsequent thermal treatments in air between 200 and 600 °C. Titania xerogels were prepared from $Ti(OPr^i)_4$ by SG dip-coating and successively used as substrates

for Au sputtering in Ar plasmas, at temperatures as low as 60 °C. The very low deposition temperature was essential in order to prevent undesired xerogel modifications.

The obtained results evidenced an *active* role of the *host* titania matrix[28] in tailoring Au nanoparticle distribution, which was further influenced by the total gold content. Au/TiO_2 nanosystems with gold crystal size between ≈2 and ≈15 nm were synthesized. In particular, average Au crystal dimensions depended linearly on annealing temperature and could be tailored as a function of total gold content in the *as-prepared* specimens. Annealing at $T \geq 400$ °C resulted in TiO_2 *anatase* crystallization (≈15 nm) and thermally induced coalescence of gold agglomerates, as indicated by TEM observations. Interestingly, an in-depth Au penetration in the subsurface titania layers was observed already for the *as-prepared* samples.

The above predictions agreed to a good extent with the evolution of optical spectra, i.e., the progressive development of SPR band at higher treatment temperatures, and the observed variations of sample surface topography, i.e., grain coarsening and surface roughening.

Further interesting perspectives for the development of this work can be envisaged. In particular, the influence of gold-titania aging at room temperature on gold coalescence/distribution deserves deeper investigations. Moreover, the use of ordered *host* matrices with controlled pore size and distribution, such as mesoporous materials, and their effect on the *guest* nucleation and arrangement will be the subject of future research activities. Finally, the investigation of Au/TiO_2 nanosystem behavior in photoelectrochemical solar cells or nonlinear optical devices applications might yield interesting results for the design and development of devices with improved functional properties.

Acknowledgment. Dr. G. Bruno (IMIP-CNR, Bari, Italy) and Dr. A. Bovo (Chemistry Department, Padova University, Padova, Italy) are gratefully acknowledged for experimental assistance. The authors are also indebted with Dr. C. Sada (INFM and Physics Department, Padova University, Padova, Italy) for the thickness measurements. Thanks are also due to Consorzio OPTEL-PNR Art. 10 legge 46/1982, Italy for financial support.

CM0353308